EUROPEAN ORGANIZATION FOR NUCLEAR RESEARCH
European Laboratory for Particle Physics

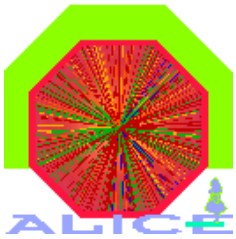

Internal Note/Physics
ALICE reference number
ALICE-INT-2005-039 version 1.0

Date of last change
26.04.2006

Reconstruction of $K^*(892)^0$ signal in ALICE using PYTHIA and HIJING event generators

Authors:

A. Badalà[1], R. Barbera[1,2], G. Lo Re[3],
G. S. Pappalardo[1], A. Pulvirenti[1,2], F. Riggi[1,2]

For the ALICE Collaboration

[1] *INFN, Sezione di Catania – Via S. Sofia, 64 I-95123 Catania (Italy)*
[2] *Dipartimento di Fisica e Astronomia dell'Universit`a di Catania, Via S. Sofia, 64 I-95123 Catania (Italy)*
[3] *CNAF, Viale Berti Pichat, 6/2, I-40127 Bologna – Italy*

Abstract:

The ability of the ALICE detector to reconstruct the $K^*(892)^0$ resonance in p-p collisions at 14 TeV and in Pb-Pb collisions at 5.5 ATeV has been investigated. PYTHIA events for p-p collisions and HIJING events for Pb-Pb collisions have been generated and fully reconstructed. The $K^*(892)^0$ was identified by its hadronic decay into πK pairs and through the invariant mass spectrum. The combinatorial background has been evaluated by the event-mixing technique for the p-p events and by the like-sign technique for the Pb-Pb events. In Pb-Pb events particular attention has been devoted to the background estimation. Moreover the role of particle identification of the decay products is discussed.

1 Introduction

The main motivation for studying heavy-ion collisions at ultrarelativistic energies is to investigate the properties of the strong interacting matter at high density and temperature. In-medium modification of meson resonances has been proposed as a possible signal of a phase transition of nuclear matter to a plasma of quarks and gluons [1]. However, even in absence of a phase transition, modifications of the properties of meson resonances can arise due to interactions of such particles and/or their daughters with the fireball medium [2-3]. The typical lifetime of such resonances is a few fm/c, which is comparable to the expected lifetime of the hot and dense matter produced in ultrarelativistic heavy-ion collisions. Then the study of these resonances may give information about its dynamics and its chiral property.

As the partonic system created in the initial stage of the ultrarelativistic collision expands and cools down, it will hadronize and chemically freeze-out. After a period of hadronic interactions, the system reaches the kinetic freeze-out stage when all hadrons stop interacting. After the kinetic freeze-out, particles free-stream towards the detectors. Study of short-lived resonances may also probe the role of the rescattering phase between chemical and kinetic freeze-out. Resonance measurements are affected by two competing effects. Some of them may not be reconstructed due to the rescattering of their daughter particles. This effect depend on the time between chemical and kinetic freeze-out, the source size, the resonance phase-space distribution and the hadronic interaction cross-section of the daughters of the resonances. However, after chemical freeze-out, pseudo-elastic interactions among hadrons in the medium may increase the resonance population. This regeneration mechanism depends on the cross-section of hadrons in the medium. Thus, the study of resonances can probe the time evolution of the source from chemical to kinetic freeze-out and test different hadronization scenarios [5].

Finally, the combined investigation of resonances with strange quark content, such as the $K^*(892)^0$ and $\phi(1020)$ mesons, is also important due to the expected overall strangeness enhancement in heavy-ion collisions [6].

The observation of such resonances is critical in heavy-ion experiments, because of the large background originating from the high multiplicity and from detector limitations. Among the most recent results, the NA49 Collaboration has reported an experimental study of the $\phi(1020)$, $K^*(892)^0$ and $\Lambda(1520)$ in Pb–Pb at $\sqrt{s} = 17.2$ GeV detected through their hadronic decay channels [7, 8]. The $\phi(1020)$, $\rho(770)$, $f(980)$, $\Delta(1232)$, $\Lambda(1520)$, $\Sigma(1385)$, $K^*(892)^{0\pm}$ resonances have been measured by the STAR Collaboration at the RHIC energies [9-17]. Yields and transverse mass spectra of $K^*(892)^0$ produced in p-p and Au-Au at $\sqrt{s} = 130$ GeV and 200 GeV have been reported in [18, 19].

Reconstruction of such resonances for Pb–Pb collision at LHC energies will be challenging due to the expected high multiplicity environment. Here a simulation study of the $K^*(892)^0$ signal in pp and Pb–Pb collisions is discussed. First results on this topic were published in [20, 21]. The $K^*(892)^0$ meson resonance and its antiparticle decay into $K\pi$, with a $c\tau$ around 4 fm/c and full width $\Gamma = (50.7 \pm 0.6)$ MeV [22]. Their decay

products may therefore be considered as originating from the primary vertex as far as the tracking is concerned. The selection of the $K^*(892)^0$ decay channel into charged particles is performed by the πK invariant mass spectrum. Great care has to be paid in the background estimate.

In Section 2 the reconstruction procedure of the $K^*(892)^0$ in pp collisions will be discussed. Section 3 will present the results obtained for central Pb–Pb collisions. The role of particle identification of the decay products will be analyzed in both cases. Conclusions will be drawn in section 4.

2 Proton-proton collisions

In order to study the $K^*(892)^0$ signal in pp collisions, a sample of 2×10^5 PYTHIA [23] (version 6.203) pp minimum bias events at $\sqrt{s} = 14$ TeV was generated and fully reconstructed; this amount of data corresponds to $\sim 10^{-2}\%$ of one year of data-taking ($2{\times}10^9$ events for a luminosity of $3{\times}10^{30}\mathrm{cm}^{-2}\mathrm{s}^{-1}$ [24]). A magnetic field of 0.4 T was used for the L3 magnet. Particles were considered over the whole solid angle and in the full momentum range. All ALICE subdetectors, together with the beam pipe, were included in the simulation, and all physical processes were switched on in GEANT.

The average $K^*(892)^0$ multiplicity, as generated by PYTHIA, is in the order of 1.7 per event (i. e. 3.4 for both $K^*(892)^0$ and its antiparticle), whereas the number of possible $K^+\pi^-$ combinations is in the order of 70 per event. After the reconstruction process the number of findable candidates (i.e. $K^*(892)^0$ for which the pion and kaon tracks have been reconstructed) is about 0.02 per event and the $K^+\pi^-$ combinations are reduced to about 1.4 per event. This strong decrease is due to several factors as: the geometrical acceptance of the TPC ($|\eta| \leq 0.9$), the branching ratio of the $K^*(892)^0$ decay into charged $K\pi$ pairs (1/3 of $K^*(892)^0$ decays into neutral πK pairs) and the tracking efficiency, especially for low momentum particles and for charged kaons which decay inside the TPC volume.

2.1 Results for a perfect particle identification efficiency

We first assumed to have a 100% efficiency for particle identification (PID); the effect of misidentifying the decay products will be discussed later. Under such conditions, the true signal obtained from a proper correlation of the true πK pairs is shown in the left panel of Fig. 1. Both $K^*(892)^0$ and its antiparticle were included in the plot, by summing $K^+\pi^-$ and $K^-\pi^+$ pairs. Fitting this peak with a Breit-Wigner function gives a centroid at $M = (897.6 \pm 0.9)$ MeV/c^2, and a width $\Gamma = (52.8 \pm 2.1)$ MeV/c^2, which are compatible with the standard PDG values ($M_{PDG} = (896.10 \pm 0.27)$ MeV/c^2, $\Gamma_{PDG} = (50.7 \pm 0.6)$ MeV/c^2) [22].

The decay products from the $K^*(892)^0$ are embedded in a sample of primary tracks, with a signal-to-background ratio S/B = 0.1, calculated within $\pm 2\sigma$ with respect to the nominal $K^*(892)^0$ invariant mass, and a significance $\mathrm{S}/\sqrt{\mathrm{S}+\mathrm{B}}$ equal to 18.0 for the number of events used in the present analysis. A fit of the unlike-sign $K\pi$ invariant mass

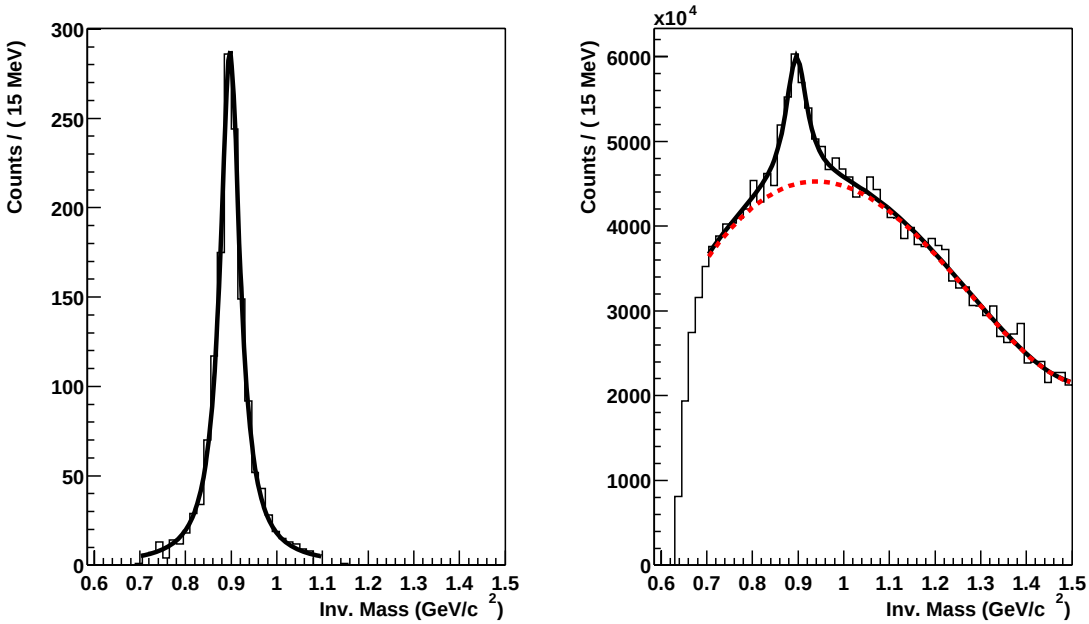

Figure 1: Invariant mass distribution of the true pairs originating from the $K^*(892)^0$ and its antiparticle decay (left panel) and from all charged $K\pi$ pairs (right panel) in the case of a perfect particle identification, for 2×10^5 PYTHIA pp collisions. The solid curves are the fit results. The dashed curve in the right part is the polynomial function representing the background.

distribution (Fig. 1, right panel) carried out with the sum of a 5th order polynomial plus a Breit-Wigner function, gives a centroid at $M = (896.3 \pm 2.6)$ MeV/c^2 and a width $\Gamma = (57.2 \pm 8.6)$ MeV/c^2 for the $K^*(892)^0$ peak, values still compatible with the nominal ones, although with a large uncertainty in the width.

These results show that with a perfect particle identification, the $K^*(892)^0$ signal may be extracted even with a limited number of events.

2.2 Results for a realistic particle identification efficiency

In the standard ALICE particle identification PID weights for each track are estimated in each individual detector; these weights are then combined in a Bayesian way [26]. Concerning a realistic particle identification, two cases were considered. In the first case, to maximize the number of tracks, the PID information was required from at least one of the three detectors ITS, TPC and TOF, while in the second case, to improve the performance, PID information was required by all the three detectors.

PID efficiency is defined as the ratio between the number of identified tracks and the overall number of tracks, while the fake probability is given by the ratio between the number of misidentified tracks and the overall number of tracks. PID efficiency and fake probability for all the tracks are shown in Fig. 2 as a function of the momentum, for

the first case. With this choice a larger misidentification is apparent for high momenta. This is especially true for kaons.

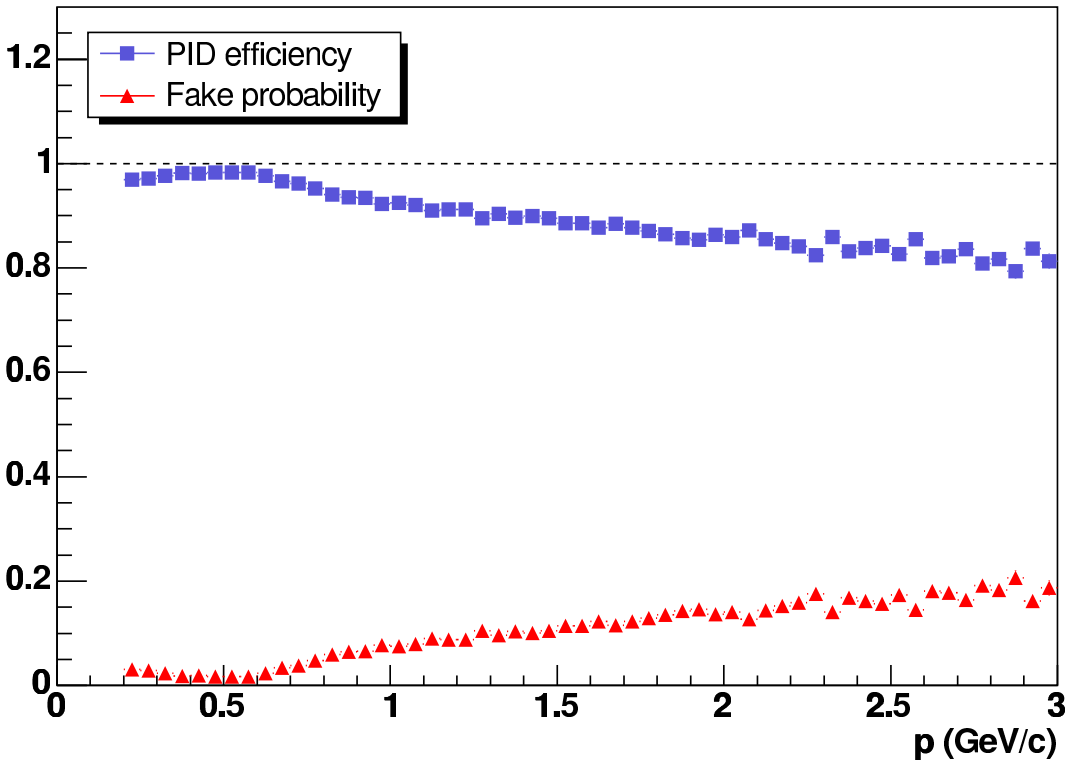

Figure 2: PID efficiency and fake probability as a function of the track momentum for the first case for PID described in the text.

A $K^*(892)^0$ is labelled as 'findable' if both its two daughters have been tracked, while it is labelled as 'good' if both the daughters have been tracked and correctly identified. In the first case for PID, the number of findable $K^*(892)^0$ is 0.02/event and the number of good $K^*(892)^0$ is 0.015/event. This results in a signal to noise ratio S/B = 0.08 within $\pm 2\sigma$ with respect to the nominal $K^*(892)^0$ invariant mass and a significance of 14. The invariant mass distribution for $K^+\pi^-$ and $K^-\pi^+$ combinations is shown in the left panel of Fig. 3.

The background was evaluated by means of the event mixing technique and subtracted from the $K\pi$ invariant mass distribution. Both $K^+\pi^-$ and the $K^-\pi^+$ combinations were included. The number of event pairs was chosen in order to have a negligible statistical error on the combinatorial spectrum. Since the multiplicity fluctuations in pp collisions may be relatively large, we mix only events whose multiplicities differ not more than 5 units. However we verified by a Kolmogorov test that very similar combinatorial spectra are obtained when event pairs whose multiplicities differ not more than 5 units or all the event pairs are considered. The normalization factor of the combinatorial spectrum to the signal spectrum was calculated taking the ratio between the number of entries in the signal and in the mixed-event distributions for invariant mass larger

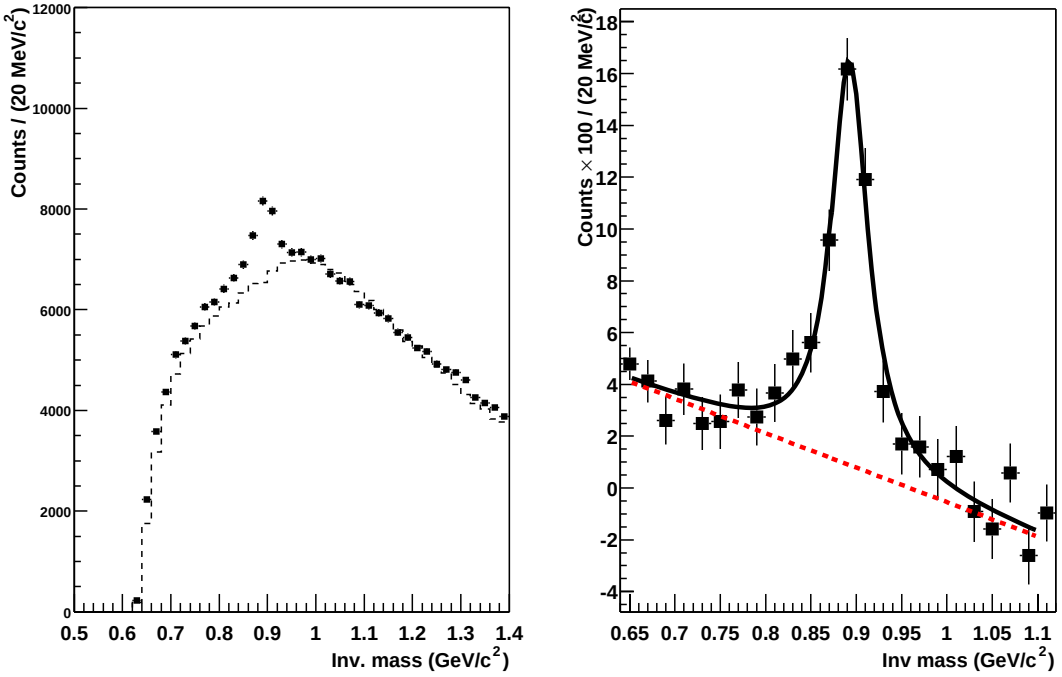

Figure 3: Left panel:invariant mass distribution of the $K^+\pi^-$ and $K^-\pi^+$ pairs in the case of a realistic PID (specified case 1 in the text); the dashed line represents the combinatorial background obtained from the event-mixing technique. The background spectrum is normalized to the entries with an invariant mass larger than $1.1\,\mathrm{GeV}/c^2$. Right panel: signal spectrum obtained after the background subtraction. The solid curve is a Breit-Wigner fit to the spectrum whereas the dashed curve is the linear function representing the residual background.

than $1.1\,\mathrm{GeV}/c^2$, since a minimum contribution from correlated Kπ pairs is expected in this range. The spectrum obtained after background subtraction (see the right panel of Fig. 3) was fitted with a Breit-Wigner function plus a linear residual background. The fit gives a mass $M = (892.6 \pm 2.1)$ MeV/c^2 and a width $\Gamma = (49.2 \pm 6.0)$ MeV/c^2.

To improve PID, although at the expense of the efficiency, PID information can be required from ITS, TPC and TOF detector together, resulting in a more regular PID efficiency as a function of the particle momenta. In this case, a track is accepted only if a PID information for it can be obtained from ITS, TPC *and* TOF: then, PID weights coming from these three detectors are combined in the Bayesian particle identification procedure. Fig. 4 shows the PID efficiency and fake track probability for kaons originating from the decay of the $K^*(892)^0$ as a function of the track momentum, in this case. The PID efficiency is defined here as the ratio of correctly identified kaons over the total number of kaon tracks for which a PID information was present in *all* the three detectors taken into account. The fake track probability is instead the ratio of the uncorrectly

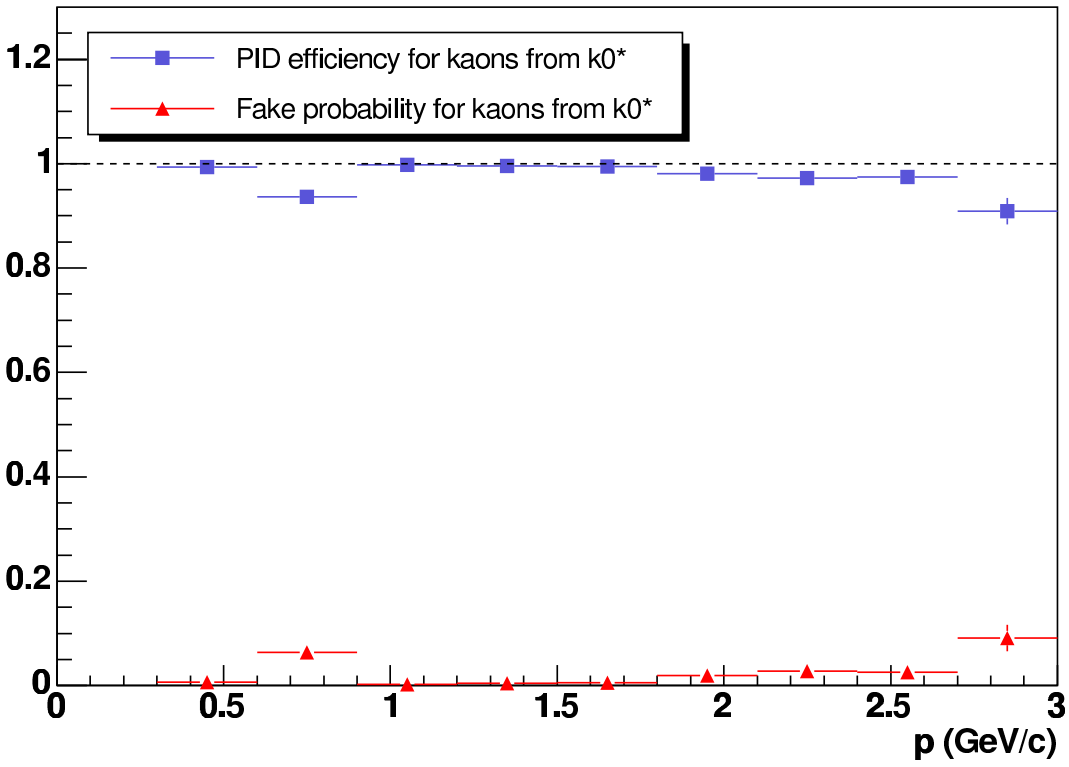

Figure 4: PID efficiency and fake probability as a function of the track momentum for kaons originating from the decay of the $K^*(892)^0$. In this case (case II in the text) particle identification from ITS, TPC and TOF is required.

identified kaon tracks over the same denominator as above.

In this specific case we define now as findable a $K^*(892)^0$ whose two daughters have been tracked and have been assigned a PID information. With such definition we found the number of findable $K^*(892)^0$ to be 0.0027/event, and the number of good $K^*(892)^0$ to be 0.0026/event. The signal-to-noise ratio is equal to 0.13 with a significance of 7.5, in the interval of invariant mass [0.8–1.0] GeV/c^2. The invariant mass distribution for both Kπ combinations is shown in the left panel of Fig. 5. Also in this case the background was evaluated by the event mixing technique and the combinatorial background was normalized to the invariant mass spectrum at $m_{inv} > 1.1\,\mathrm{GeV}/c^2$. The resulting difference spectrum between the signal and the combinatorial spectrum is reported in the right panel of Fig. 5. The fit, i. e. a combination of a Breit-Wigner curve and a linear background, gives $M = (894.5 \pm 4.0)$ MeV/c^2 and $\Gamma = (66 \pm 13)$ MeV/c^2.

We conclude that in the case of a realistic particle identification and with a number of 200,000 events, it is possible to extract values of the centroid and of the width of the resonance which are compatible with the standard values.

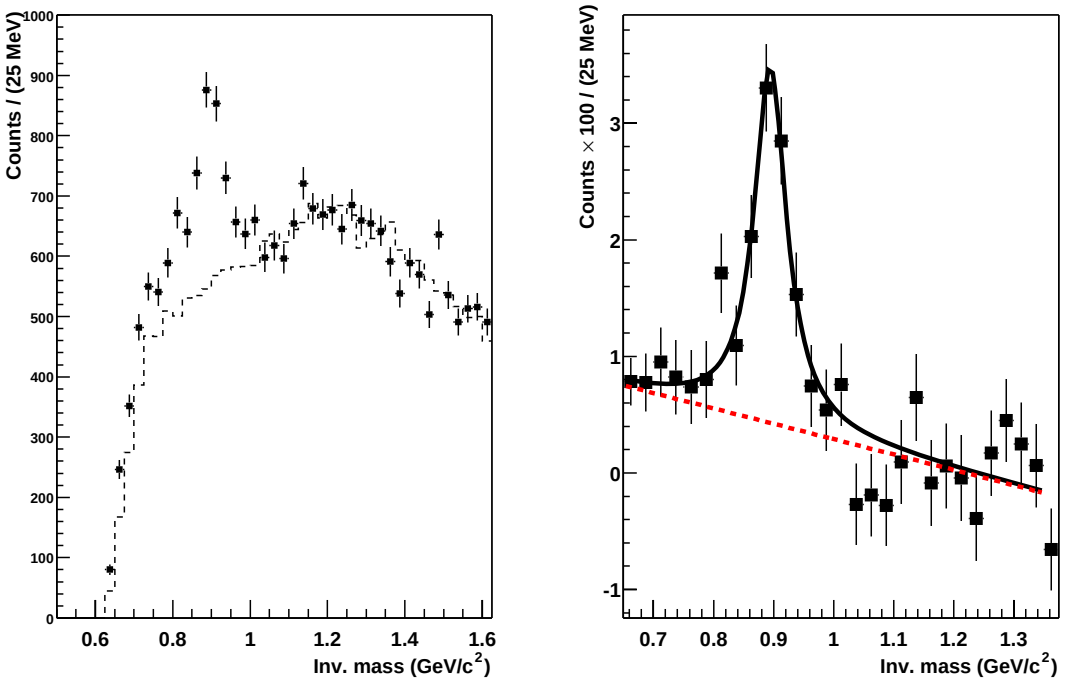

Figure 5: Left panel: invariant mass distribution of the $K^+\pi^-$ and $K^-\pi^+$ pairs, in the case of realistic particle identification (case 2 in the text); the dashed line represents the combinatorial background obtained from the mixed-event method. The background spectrum is normalized to the events with an invariant mass larger than $1.1\,\mathrm{GeV}/c^2$. Right panel: signal spectrum obtained after the background subtraction. The solid curve is the fit result. The dashed curve is the linear function representing the residual background.

3 Pb-Pb collisions

As shown in Fig. 6, the number of $K^*(892)^0$ generated in a central ($b = 3$ fm) Pb-Pb collision increases with the center of mass energy ($\sqrt{s_{NN}}$). It is in the order of 10^3 per central event in the whole solid angle at the LHC energies.

To study the ability of ALICE to detect the $K^*(892)^0$ signal in Pb-Pb collisions, two sets of events have been considered. These were produced during the Particle Data Challenge 2004. In these sets of data the magnetic field was set to 0.5 T. These events were generated and fully reconstructed. The first is a sample of 3840 central HIJING [25] events ($b \leq 5$ fm), for which a perfect particle identification was assumed. The second is a sample of 15440 central HIJING events ($b \leq 5$ fm), for which only a realistic particle identification, based on the weights calculated by a Bayesian approach during the tracking procedure, was available [26].

The $K^*(892)^0$ was identified by its hadronic decay channels: $K^*(892)^0 \rightarrow K^+\pi^-$ and $\overline{K^*(892)^0} \rightarrow K^-\pi^+$. In the following, the terms $K^*(892)^0$ stands for both $K^*(892)^0$ and

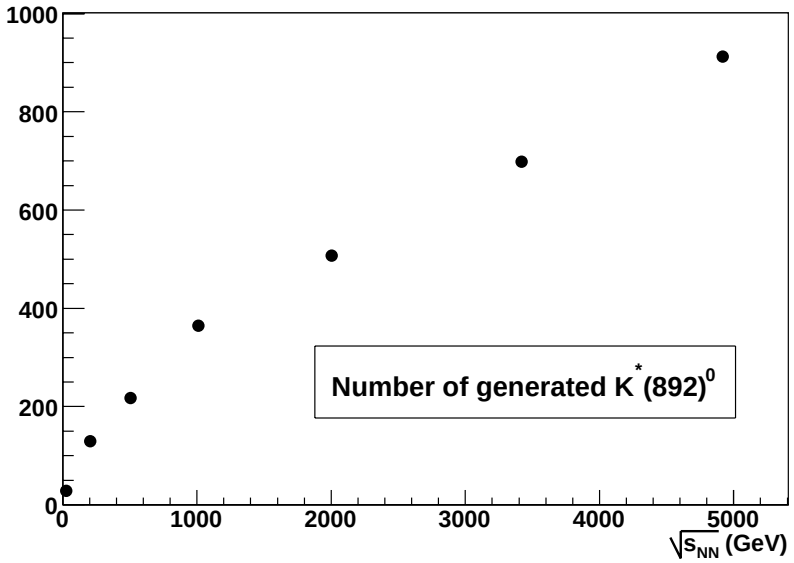

Figure 6: Number of $K^*(892)^0$ generated in Pb-Pb collisions at an impact parameter $b = 3$ fm, as a function of $\sqrt{s_{NN}}$.

its antiparticle.

Usually, to extract the real resonance width it is necessary to take into account the effective mass resolution. Fig. 7 shows the distributions of the difference between the invariant mass obtained from the original momenta and from the reconstructed ones, for different p_t bins. These curves are fitted by a gaussian function. The σ parameters (the effective mass resolution) slightly change from 3.2 to 3.0 MeV/c when p_t varies from 0.5 GeV/c to 2 GeV/c.

As already done in the case of *pp* events, the way to reconstruct the $K^*(892)^0$ signal consists in computing the invariant mass spectrum of the unlike-sign $K\pi$ pairs, and then to estimate the combinatorial background which must be subtracted from this distribution. Here, the background is calculated by sampling the like-sign pairs ($K_i^+\pi_i^+$ and $K_i^-\pi_i^-$) taken in the same event. In this way possible problems related to the event structure (as multiplicity, flow, primary vertex position) are avoided. A simple way to estimate this background is just to sum the two like-sign $K\pi$ distributions.

$$N_{\mathrm{like-sign}}(m) = N_{K_i^+\pi_i^+}(m) + N_{K_i^-\pi_i^-}(m) \tag{1}$$

Since the number of positive and negative particles may not be the same, the STAR Collaboration [18] suggested to calculate the like-sign $K\pi$ invariant mass (m) distribution as:

$$N_{\mathrm{like-sign}}(m) = 2 \times \sqrt{N_{K_i^+\pi_i^+}(m) \times N_{K_i^-\pi_i^-}(m)} \tag{2}$$

Figure 8 shows both the unlike-sign pairs and like-sign pairs invariant mass spectra estimated by equation (2), for about 3800 Pb-Pb central HIJING events at $\sqrt{s_{NN}}$ of 5.5 TeV. It is quite evident that the $K^*(892)^0$ peak is not as well visible as it was in the

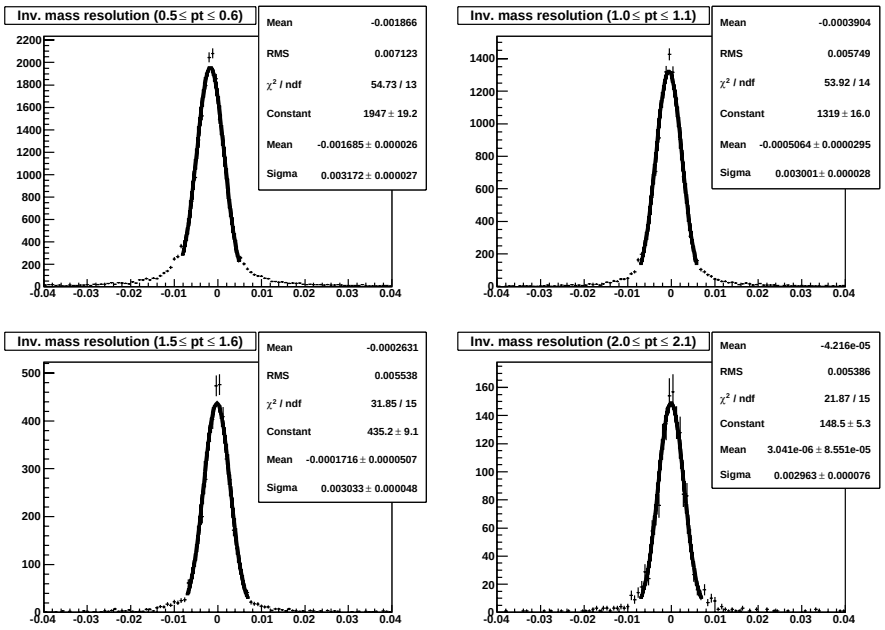

Figure 7: Mass resolution for $K\pi$ pairs of different p_t. The curves are the results of a gaussian fit.

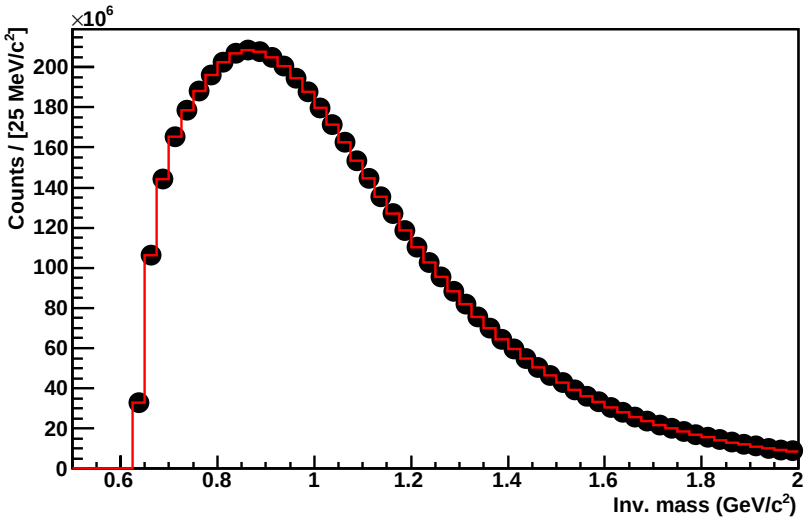

Figure 8: Invariant mass spectra of like-sign (histogram) and unlike-sign (full circles) charged $K\pi$ pairs for $\sim$ 3800 Pb-Pb central HIJING events at $\sqrt{s_{NN}}$=5.5 TeV

case of *pp* collisions. Then, in order to see the signal clearly, a good estimation of the background is required.

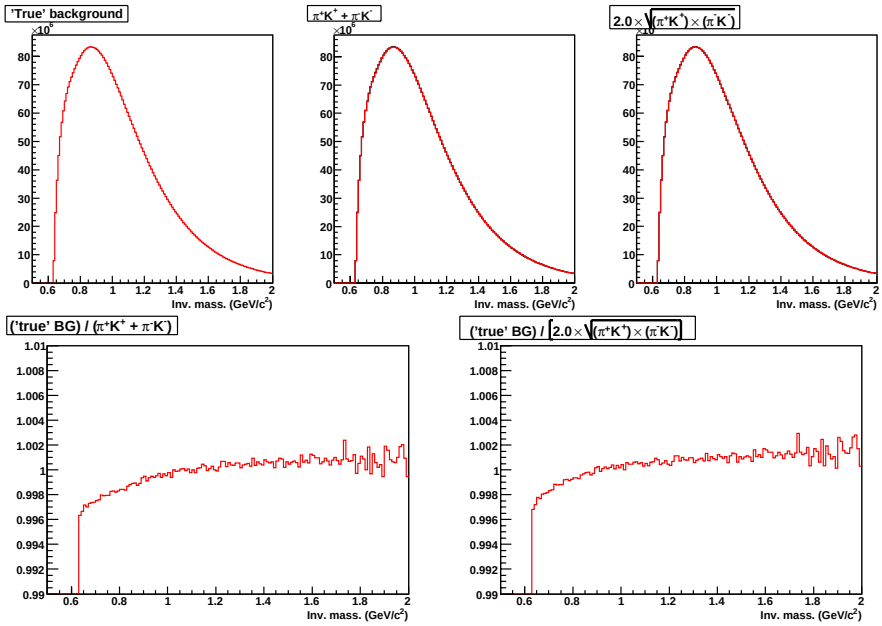

Figure 9: Upper row: "True combinatorial background" of the $K^*(892)^0$ invariant mass spectrum (see text, left panel); background of the $K^*(892)^0$ invariant mass spectrum estimated by like-sign $K\pi$ distribution of equation (1) (middle panel); background of the $K^*(892)^0$ invariant mass spectrum estimated by the like-sign $K\pi$ distribution of equation(2) (right panel). Lower row: Ratio of the "true" combinatorial background (i. e. the unlike-sign $K\pi$ pairs not coming from the $K^*(892)^0$ resonance) over the like-sign background defined by equation(1) (left panel); ratio of the "true" combinatorial background over the like-sign background defined by equation(2) (right panel);

3.1 Optimization of combinatorial background estimation

The "true" combinatorial background in the unlike-sign invariant mass distribution comes from the "false" π^+K^- and π^-K^+ pairs, i. e. the ones which are not daughters of a $K^*(892)^0$ or at least not of *the same* $K^*(892)^0$. When operating on simulated events, anyway, one can detect such "false" pairs and create their invariant mass distribution (left panel of upper row of fig. 9). Then, comparing the "true" background with the like-sign one defined by equation (1) (middle panel of upper row of Fig. 9) or by equation (2) (right panel of upper row of Fig. 9), one can evaluate how well the latters reproduce the former. Figure 10 shows the ratio between these two background evaluations. As shown, the difference between them is not constant and ranges between $5 \cdot 10^{-4}$ and 10^{-3}. The left and right panels of lower row of Fig. 9 show the ratios of the "true" combinatorial background over the like-sign background estimated by equation (1) (left panel of lower row of Fig. 9) or by(2) (right panel of lower row of Fig. 9). It is evident that in the region $m_{inv} < 1\ GeV/c^2$ the "true" and the estimated background are quite different. Then, a correction to the like-sign distribution is needed, in order to reproduce correctly the "true" background. Since in real data it is not possible to calculate the "true" background as it was done before, some other method must be used in order to

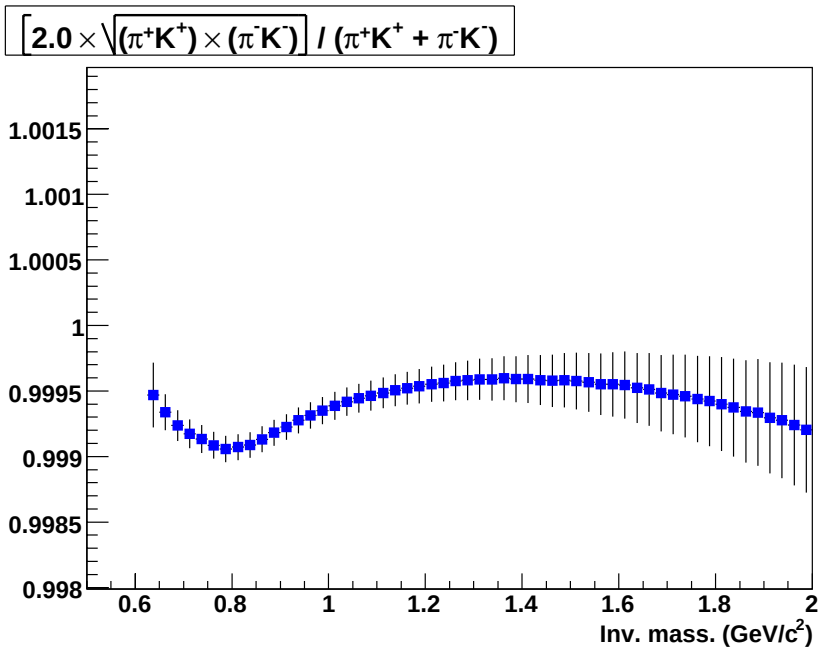

Figure 10: Ratio of the two backgrounds calculated from like sign pairs: the one calculated with equation(2) over the one calculated with equation(1)

estimate such correction.

One can consider that, in the range of the distribution outside the $K^*(892)^0$ resonance peak ($\pm 2\Gamma_{PDG}$), the contribution of the $K^*(892)^0$ daughters is almost negligible. In fact, in the interval of m_{inv} $(0.7 - 0.8)$ GeV/c^2 or $(1.0 - 1.1)$ GeV/c^2 the ratio (number of K*)/(number of background pairs) is roughly equal to 0.0016 %. Then, it is possible to conclude that the unlike-sign pair distribution, in the ranges outside the interval $[0.8 - 1.0]$ GeV/c^2 is made essentially of "false" pairs. It is then possible to compute the ratio of unlike-sign to like-sign distribution just in these ranges (i. e. outside the invariant mass interval where the peak is present), in order to estimate experimentally the ratio of "true" background to like-sign distribution.

Figure 11 shows the result of this operation. As it is possible to observe, this ratio has a smooth increase in the small invariant mass range, while becomes almost flat when m_{inv} increases. It is also quite similar to the ratio shown in Fig. 9. The curve shown in figure is the result of a 4th order polynomial fit. This polynomial line can be used as a correction term for the like-sign spectrum. This improved estimation of the background allows to see the $K^*(892)^0$ peak, and it does not take into account any information from simulation. We verified also that the difference between this and the "true" correction (i.e. the correction obtained fitting the ratio between the "true" and the like-sign distribution), for invariant mass values in the range [0.65-1.2] GeV/c, is always less than 5×10^{-4}.

Left panel of Fig. 12 shows the result of the subtraction of the uncorrected like-sign background, estimated by equation (2), from the unlike sign spectrum, while right panel shows the result of the same subtraction, but with the corrected background. In

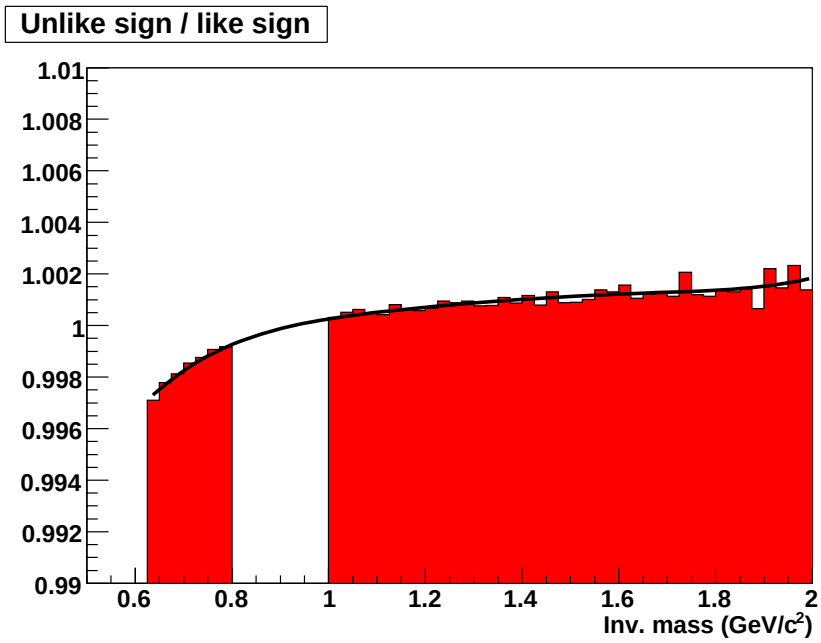

Figure 11: Ratio of the unlike-sign combinatorial background over the like-sign background defined in equation (2), in the region outside the $K^*(892)^0$ peak.The line is the result of a polynomial fit.

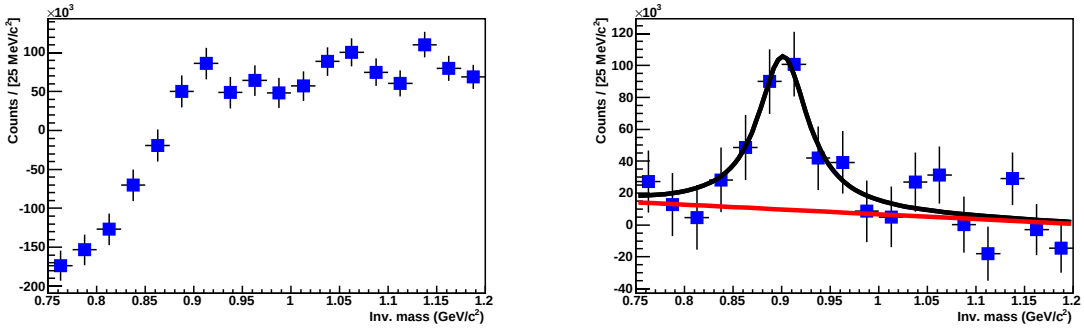

Figure 12: Left panel: result of the subtraction of uncorrected like-sign distribution from unlike sign one. Right panel: result of the subtraction of corrected like-sign distribution from unlike sign one.

the second case, the $K^*(892)^0$ peak becomes clearly visible, even if a residual linear background is still present.

In the further analysis of the extraction of $K^*(892)^0$ peak this correction was then always applied to the data.

We noticed also that this correction is needed only for low-p_t K*. In Fig. 13, the ratio beetwen the "true background" and the background estimated by equation (2) is shown for different p_t bins. Then the correction to the background is more important for $K^*(892)^0$ with p_t smaller than 1 GeV/c.

To understand the origin of this kind of correction we make the same analysis on the

"original" HIJING particles. We found that the ratio between the "true" background and the like-sign distribution is equal to one in the regions of m_{inv} external to the $K^*(892)^0$ resonance (see Fig. 14). Then the previously described correction to the background estimated by the like-sign pairs invariant mass distribution is mostly an effect of the reconstruction phase.

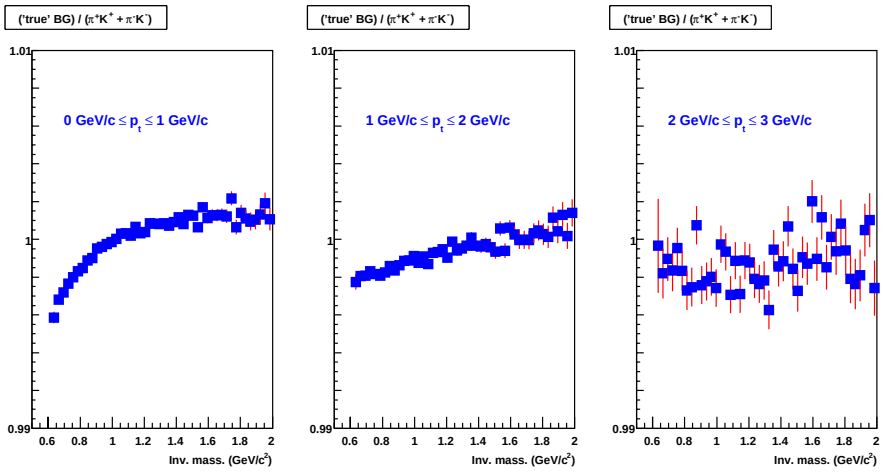

Figure 13: Ratio of the true combinatorial background over the like-sign background defined in equation 2 for different p_t range of the Kπ pairs

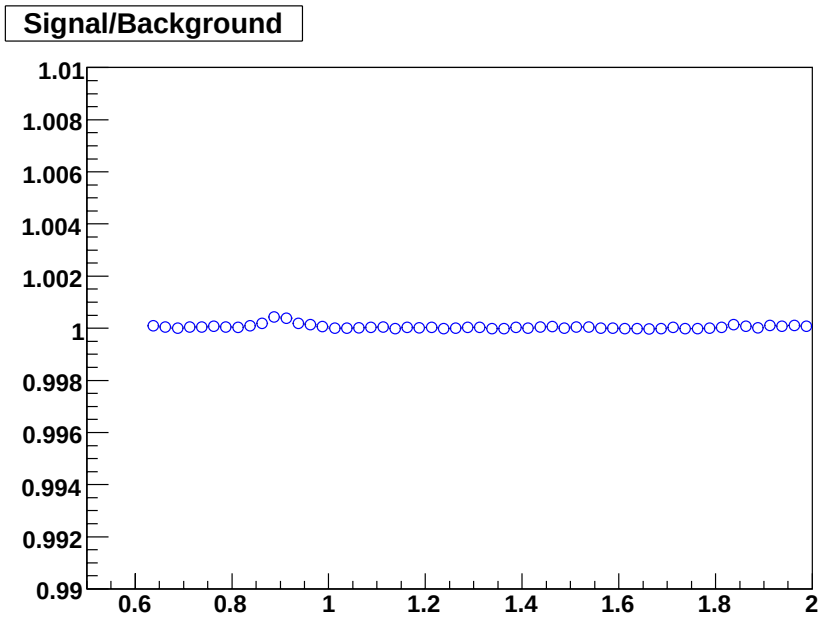

Figure 14: Ratio of the true combinatorial background over the like-sign background defined in equation 2 for the original HIJING particles.

p_t bin (GeV/c)	S/B	$\frac{S}{\sqrt{S+B}}$ (I)	$\frac{S}{\sqrt{S+B}}$ (II)
$0.0 \div 1.0$	2.4×10^{-4}	6.5	331.6
$1.0 \div 2.0$	3.1×10^{-4}	4.0	201.4
$2.0 \div 3.0$	1.1×10^{-3}	2.8	145.4
$3.0 \div 4.0$	2.8×10^{-3}	2.3	118.0
$4.0 \div 5.0$	4.8×10^{-3}	1.9	98.4
$5.0 \div 6.0$	6.2×10^{-3}	1.4	72.2
$6.0 \div 7.0$	8.5×10^{-3}	1.2	60.1

Table 1: S/B (second column) and significance (third column) for different bins in total transverse momentum p_t of $K^*(892)^0$ in the case of perfect particle identification, for the about 3800 HIJING Pb–Pb events. Rightmost column reports the significance scaled by the expected number of central events collected after 1 year of data-taking ($\simeq 10^7$).

3.2 Results for a perfect PID efficiency

Results presented in this Section were obtained with the already described 3840 central HIJING events, with perfect PID. This ideal PID is possible in the simulation.

Table 1 shows S/B, calculated within $\pm 2\sigma$ around the nominal value of the $K^*(892)^0$ mass, and the significance obtained with the sample of events used for this study, calculated for different bins in the total transverse momentum p_t of the pair. For each bin, a significance estimation is made also for a number of 10^7 events, i. e. the estimated amount of central events which ALICE should collect after 1 year of data taking (= 1 month of Pb-Pb data taking).

In this sample of events $\sim 2100 K^*(892)^0$ are generated per event. A $K^*(892)^0$ is considered findable if both its daughter particles were reconstructed; the number of findable $K^*(892)^0$ drops down to ~ 67/event after reconstruction. The global signal to background ratio is S/B $(\pm 2\sigma)) \simeq 10^{-4}$.

Figure 15 shows the $K^*(892)^0$ peak obtained from the subtraction of the background from the distribution of unlike-sign $K\pi$ pairs, with the method described in Section 3.1, when limiting the study to total transverse momentum smaller than 1 GeV/c. A fit of the $K\pi$ effective mass spectrum using a Breit-Wigner function plus a linear background gives reasonable results for the centroid and the width of the resonance peak.

The global reconstruction efficiency (including geometrical acceptance, branching ratio and tracking efficiency) is shown in fig. 16 as a function of the transverse momentum. It ranges from about 4% for $p_t \leq 1$ GeV/c to about 11% for p_t equal to 6 GeV/c.

3.3 Results for a realistic particle identification

Table 2 shows, for the 3840 HIJING events, the S/B ratio and the significance for different p_t bins, together with an extrapolation of significance in the case of 1 year of data taking in the case of a realistic particle identification based on the Bayesian weights calculated during the tracking procedure. According to the standard reconstruction

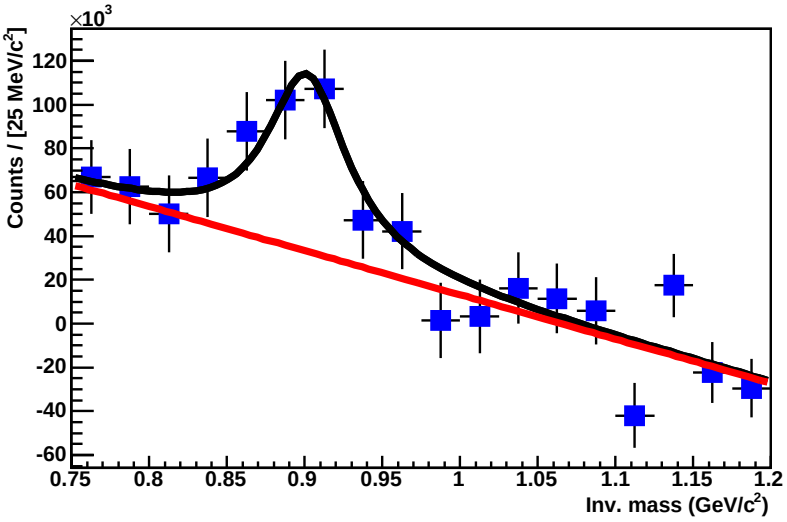

Figure 15: $K^*(892)^0$ resonance peak obtained after subtraction of like-sign background (corrected as described in the text), for 3840 Pb-Pb HIJING events, with a perfect PID, for $p_t \leq 1\,\mathrm{GeV}/c$. The curve represents the result of a fit by a Breit-Wigner plus a linear background.

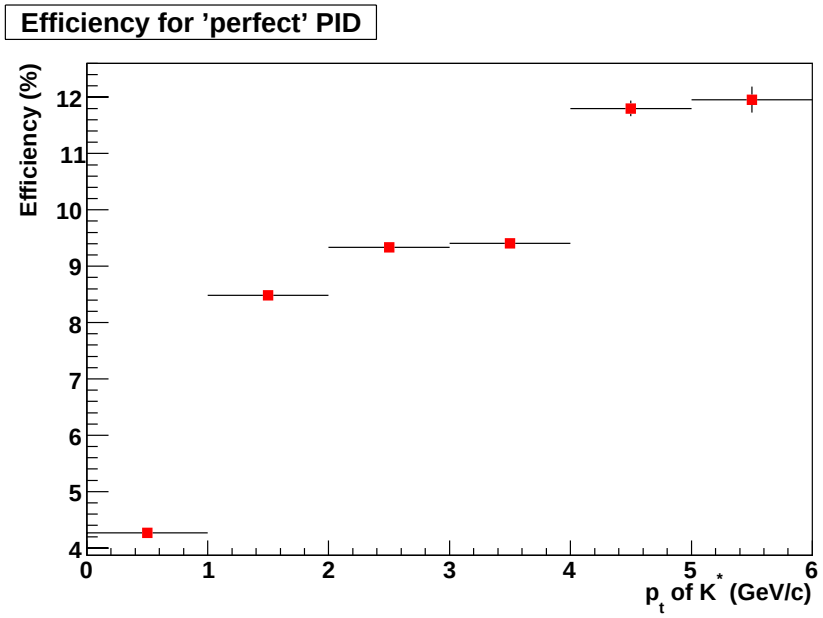

Figure 16: Global reconstruction efficiency as a function of the K^* transverse momentum in the case of a perfect particle identification.

procedure, each track is read by means of the corresponding `AliESDtrack` object, which contains also the PID weights related to the probability to be one of the most common charged particles (e, μ, π, K or p). Combining these weights with suitable estimates of the prior probability for each of these particles to be produced (which can be estimated by simply comparing the relative abundances of reconstructed particles), it is possible to

p_t bin (GeV/c)	S/B	$\frac{S}{\sqrt{S+B}}$ (I)	$\frac{S}{\sqrt{S+B}}$ (II)
$0.0 \div 1.0$	1.9×10^{-4}	4.9	252.1
$1.0 \div 2.0$	2.3×10^{-4}	2.6	130.0
$2.0 \div 3.0$	9.8×10^{-4}	1.7	86.6

Table 2: S/B (second column) and significance (third column) for different bins in total transverse momentum p_t of $K^*(892)^0$ in the case of realistic particle identification, for 3840 HIJING Pb–Pb events. Rightmost column reports the significance scaled by the expected number of central events collected after 1 year of data-taking ($\simeq 10^7$).

evaluate the probability for each track to have been produced by one of these particles. Each track is then identified as if it has been produced by the particle type to which corresponds the largest probability, according to the Bayesian combination of PID weights and prior probabilities.

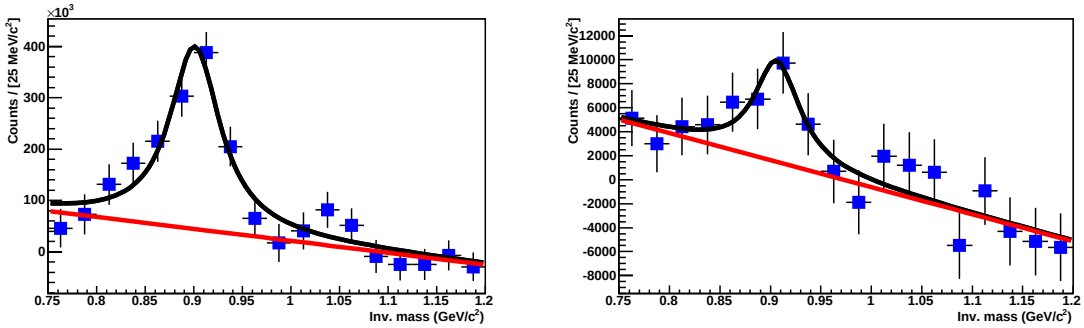

Figure 17: $K^*(892)^0$ resonance peak obtained after subtraction of like-sign background (corrected as described in the text), for 15000 Pb-Pb central HIJING events, with realistic PID. Left panel: result for the whole p_t range. Right panel: result for $2\,\mathrm{GeV}/c \leq p_t \leq 3\,\mathrm{GeV}/c$ range. In both plots, the curve represents the result of a fit by a Breit-Wigner plus a linear background.

In order to evaluate the visibility of the peak in a more realistic scenario, another sample of 15440 central HIJING events fully reconstructed was used. The $K^*(892)^0$ resonance peak is then extracted in the same way as before, by creating the unlike-sign pairs invariant mass distribution, and subtracting from it the like-sign pairs invariant mass distribution, corrected as described in Section 3.1. Figure 17 shows the result: left panel shows the calculation in the whole p_t range, and right panel shows the calculation for $2\,\mathrm{GeV}/c \leq p_t \leq 3\,\mathrm{GeV}/c$ only. Also in this case, the peak is clearly visible and a fit by a Breit-Wigner distribution plus a linear background gives reasonable results for the centroid and the width of the resonance peak.

The global reconstruction efficiency (including geometrical acceptance, branching ratio, tracking efficiency and particle identification efficiency) as a function of the transverse momentum is shown in Fig. 18. In this case the efficiency has a maximum at about 4% for p_t equal to 1.5 GeV/c, decreasing smoothly to 1.2 % for p_t equal to 5.5 GeV/c.

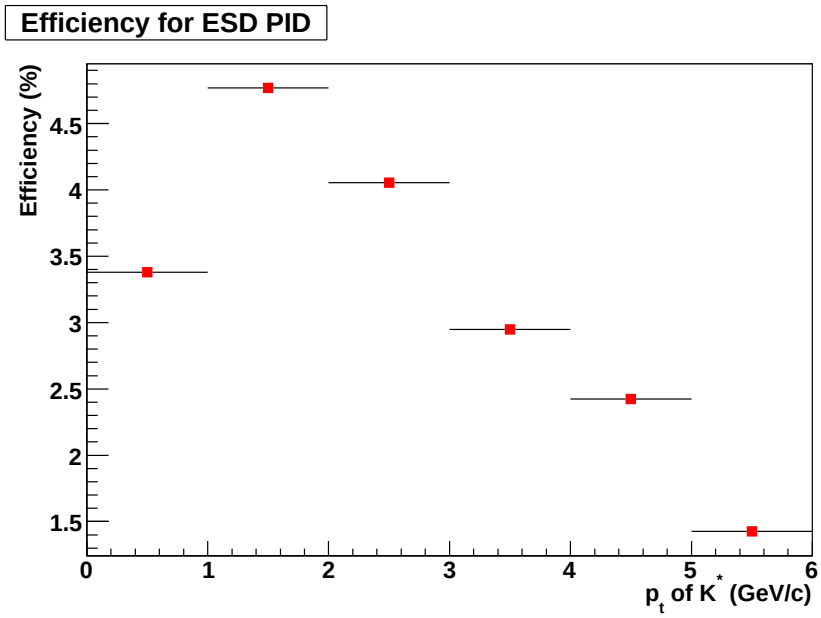

Figure 18: Global reconstruction efficiency as a function of the K^* transverse momentum in the case of a realistic particle identification.

4 Conclusions

A study of the extraction of $K^*(892)^0$ resonance peak in pp and PbPb collisions at LHC has been described. The $K^*(892)^0$ is identified by its hadronic decay into charged πK pairs by their invariant mass spectrum. A realistic simulation and reconstruction has been done using about 200,000 minimum-bias PYTHIA events for p-p collisions and about 15,000 central HIJING events for Pb-Pb collisions. Studies of the extraction of this signal have been done both in the case of a perfect particle identification efficiency and in the case of a realistic one. For both systems, results show that the resonance peak is detectable with such number of events. Great care has been devoted to the estimation of the combinatorial background. This has been evaluated by the event-mixing technique for the p-p events and by the like-sign technique for the Pb-Pb events. In the latest it was necessary to apply a small correction to the background spectrum estimated by the like-sign technique. This correction depends on the p_t of the πK pair and it is an effect of the reconstruction phase. A procedure to evaluate it by the experimental data has been tested.

The analysis reported in this Note has been performed using the present ALICE PID. Improvements in the PID for high momentum particles (studies on the relativistic rise in the TPC have been started [27]) would be of great help in the identification of intermediate and high transverse momentum resonances, whose nuclear form factors as a transverse momentum function have been extensively studied by the RHIC experiments, showing strong differences between mesons and baryons and allowing to study the interplay between recombination and fragmentation models [28].

References

[1] R. Rapp and J. Wambach, Adv. Nucl. Phys. **25** (2000), 1
R. Rapp, Phys. Rev. **C63** (2001), 054907.

[2] E.V. Shuryak and G.E. Brown, Nucl. Phys. **A717** (2003), 322.

[3] R. Rapp, Nucl. Phys. **A725** (2003), 254.

[4] M. Bleicher and H. Stocker, J. Phys. **G30** (2004), S111.

[5] J. Letessier *et al.*, J. Phys. **G27** (2001), 427
G. Torrieri and J. Rafelski, Phys. Lett. **B509** (2001), 239.

[6] J. Rafelski and B. Muller, Phys. Rev. Lett. **48** (1982), 48
Phys. Rev. Lett. **56** (1985), 2334.

[7] V. Friese for the NA49 Collaboration, Nucl. Phys. **A698** (2002), 487c.

[8] S. V. Afanasiev *et al.* (NA49 Collaboration), Phys. Lett. **B491** (2000), 59.

[9] J. Adams *et al.* (STAR Collaboration), Phys. Lett. **B612** (2005), 181.

[10] J. Adams *et al.* (STAR Collaboration), Phys. Rev. Lett. **92** (2004), 092301.

[11] C. Adler *et al.* (STAR Collaboration), Phys. Rev. **C65** (2002), 041901.

[12] S. Salur for the STAR Collaboration, Eur. Phys. J. **40** (2005), 9.

[13] C. Market for the STAR Collaboration, J. Phys. **G30** (2004), S1313; Heavy-Ion Phys. 21(2004), nucl-ex/0308029.

[14] H. Zhang for the STAR Collaboration, nucl-ex/0403010

[15] S. Salur for the STAR Collaboration, hep-ex/0403016, Proceedings of Camyuvakermer 2003, Structure and dynamics of elementary matter, p. 665.

[16] L. Gaudichet for the STAR Collaboration, J. Phys. **G30** (2004), S549.

[17] P. Fachini for the STAR Collaboration J. Phys. **G30** (2004), S565.

[18] J. Adams *et al.* (STAR Collaboration) Phys. Rev. **C71** (2005), 064902.

[19] C. Adler *et al.* (STAR Collaboration), J. Phys. **G28** (2002), 1599
and Phys. Rev. **C66** (2002), 061901.

[20] A. Badalà *et al.*, ALICE Internal Note ALICE/INT 2003-31.

[21] A. Badalà *et al.*, Nucl. Instr. and Meth. in Phys. Res. **A534** (2004), 189.

[22] Particle Data Group, K. Hagiwara *et al.*., Phys. Rev. **D66** (2002), 010001.

[23] H. U. Bengtsson and T. Sjostrand, Comput. Phys. Comm. **46** (1987), 43

[24] ALICE Physics Performance Report Vol. I, ALICE Collaboration, J. Phys. **G30** (2004), 1517.

[25] H. Giulassy and X.N. Wang, Comput. Phys. Comm. **83** (1994), 307.

[26] I. Belikov *et al.*, Proceedings of CHEP 2004, Interlaken, Switzerland, (2004).

[27] P. Christiansen and J. Baecheler, ALICE Internal Note ALICE/INT 2005-30.

[28] J. Adams *et al.* (STAR Collaboration) Nucl. Phys. **A757** (2005), 102.